Internal quantum efficiency of radiation in a bulk CH3NH3PbBr3 perovskite crystal quantified by using the omnidirectional photoluminescence spectroscopy

AUTHOR(S):

Kojima, K.; Ikemura, K.; Matsumori, K.; Yamada, Y.; Kanemitsu, Y.; Chichibu, S. F.

CITATION:

Kojima, K. ...[et al]. Internal quantum efficiency of radiation in a bulk CH3NH3PbBr3 perovskite crystal quantified by using the omnidirectional photoluminescence spectroscopy. APL Materials 2019, 7(7): 071116.

ISSUE DATE:

2019-07

URL:

http://hdl.handle.net/2433/243259

APL Materials

Internal quantum efficiency of radiation in a bulk $CH_3NH_3PbBr_3$ perovskite crystal quantified by using the omnidirectional photoluminescence spectroscopy

Cite as: APL Mater. **7**, 071116 (2019); https://doi.org/10.1063/1.5110652
Submitted: 20 May 2019 . Accepted: 01 July 2019 . Published Online: 31 July 2019

K. Kojima, K. Ikemura, K. Matsumori, Y. Yamada, Y. Kanemitsu, and S. F. Chichibu

APL Materials ARTICLE scitation.org/journal/apm

Internal quantum efficiency of radiation in a bulk $CH_3NH_3PbBr_3$ perovskite crystal quantified by using the omnidirectional photoluminescence spectroscopy

Cite as: APL Mater. 7, 071116 (2019); doi: 10.1063/1.5110652
Submitted: 20 May 2019 • Accepted: 1 July 2019 •
Published Online: 31 July 2019

K. Kojima,[1] K. Ikemura,[2] K. Matsumori,[3] Y. Yamada,[3] Y. Kanemitsu,[4] and S. F. Chichibu[1]

AFFILIATIONS

[1]Institute of Multidisciplinary Research for Advanced Materials, Tohoku University, Aoba, Sendai 980-8577, Japan
[2]Applied Spectroscopy Systems Department, Hamamatsu Photonics K. K., Higashiku, Hamamatsu 431-3196, Japan
[3]Graduate School of Science, Chiba University, Inage, Chiba 263-8522, Japan
[4]Institute for Chemical Research, Kyoto University, Gokasho, Uji 611-0011, Japan

ABSTRACT

The internal quantum efficiency (IQE) of radiation for bulk $CH_3NH_3PbBr_3$ crystals was quantified by using omnidirectional photoluminescence spectroscopy. The angle-resolved photoluminescence revealed that the emission with photon energies higher than the absorption-edge shows a Lambertian distribution and that the light extraction efficiency is determined by the escaping cone. The IQE value strongly depends on the photo-excitation density (P), and a $CH_3NH_3PbBr_3$ crystal fabricated under the methylammonium-rich conditions gave the maximum IQE of 62.5% under $P = 28$ W/cm^2. A further increase in P gave rise to the decrease in IQE due to the Auger effects.

I. INTRODUCTION

Lead halide perovskite $APbX_3$ [A = CH_3NH_3 (MA), $CHNH_2$, Cs; X = I, Br, Cl] is a promising class of semiconductor materials for application to solar cells as well as light-emitting devices and detectors because of their excellent optical properties originating from long lifetime of photo-excited carriers.[1–14] Due to the strong tolerance to structural defects, $APbX_3$ exhibits small nonradiative recombination rate and results in a high internal quantum efficiency (IQE), which are the key feature not only for the wall-plug efficiency of light-emitting devices but also for the conversion efficiency in solar cells.[15,16] Recent discovery of the photon recycling effect supported by the high IQE in $APbX_3$ also highlighted the significance of efficient light emission on the luminescent properties and device performance.[17–21] Laser cooling, enabling novel applications such as optical refrigerators, has also been expected based on up-converted photoluminescence (PL).[22,23] For further development of perovskite-based devices, it is essential to quantitatively evaluate the carrier recombination process and identify the limiting factor for light emission efficiency. To comply with this demand, the measurement of absolute IQE in high-quality perovskite crystals without assuming predefined physical model is of particular importance, whereas the high IQE in halide perovskites has been estimated by model-dependent analyses of PL dynamics in previous reports.[20,24]

The IQE value in matter is determined by a balance between the radiative and nonradiative recombination rates. For fluorescence particles and chemical molecules, the measurements of quantum efficiency have generally been done based on PL spectroscopy as PL quantum yield (PLQY), or equivalently, external quantum efficiency (EQE) by using an integrating sphere. The EQE value of these materials is usually recognized to be very close to the value of IQE itself owing to the large Stokes shift between absorption and emission energies in most cases. However, the number of experiments

for such EQEs as well as IQEs of solid-state light-emitters, especially for direct bandgap semiconductors, is very limited up to now. This is because EQE is a complicated function of both IQE and light extraction efficiency (LEE) in such solid-state materials in contrast to particles and molecules. Since the spontaneous emission spectra of the direct bandgap materials are usually broadened across the fundamental absorption-edge energy (E_{abs}), LEE has a significant dependence on photon energy (E), which makes the accurate estimation of LEE difficult.

To overcome this problem, the authors have recently developed the omnidirectional PL (ODPL) spectroscopy,[25] which is an experimental technique for the IQE quantification of bulk semiconductor crystals. Actually, the IQE values were quantified in direct bandgap materials such as freestanding GaN[26] and ZnO[27] crystals by this method. In this work, IQE of bulk $MAPbX_3$ crystals is measured by the ODPL method. Our results help to evaluate the potential of halide perovskites for the optoelectronic device applications.

II. SAMPLES AND EXPERIMENTAL METHODS

The bulk $MAPbBr_3$ crystals were prepared by antisolvent-vapor assisted crystallization[28] from an N, N-dimethylformamide (DMF) solution. Purified lead bromide (3 mmol) and methylammonium bromide were dissolved in dry DMF (3 ml) in small vials. Three vials were prepared that contain solutions with different MA bromide (MABr) concentrations (0.80, 1.00, and 1.25 mol/l) for comparing the IQE values. Then, these small vials were placed in a larger Teflon-capped vial containing 75 ml toluene. Through heating the vial on a hot plate for 24 h at 40 °C, clear-faceted cubic bulk crystals with a few millimeters in size were formed in the small vials. Hereafter, the samples grown with the MABr concentration of 0.80, 1.00, and 1.25 mol/l are labeled S1, S2, and S3, respectively.

Three different PL measurements were carried out, namely, standard PL (SPL), ODPL, and angle-resolved PL (ARPL) spectroscopy for the near-band-edge (NBE) emission of the samples. The SPL and ODPL measurements, schematically shown in Fig. 1, were done for the quantification of IQE as well as EQE. The numbers of input excitation photons (N_{in}), excitation photons absorbed by the sample (N_{abs}), and PL photons emitted (escaped) from the sample (N_{PL}) are independently measured by using a photodetecting system

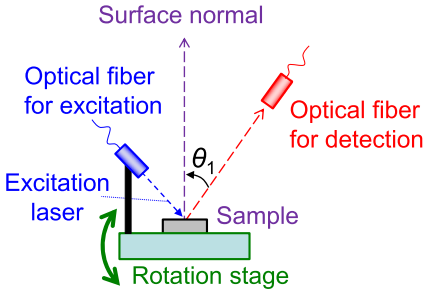

FIG. 2. Schematic of the ARPL measurement.

(C10027-01, Hamamatsu) composed of an optical fiber, a spectrometer, and a CCD camera. The absorbance of the excitation laser and EQE values can be quantified as N_{abs}/N_{in} and N_{PL}/N_{abs}, respectively. For the validity verification of the IQE quantification based on the ODPL method, ARPL spectroscopy was carried out, where the spatial distribution of PL intensity was measured, as illustrated in Fig. 2. For ODPL spectroscopy, the sample was placed in the integrating sphere (customized C9920-02, Hamamatsu) and the photodetection was done by using the measurement system via the optical fiber. A solid-state cw laser (3.06 eV) was commonly used to excite PL. All experiments were carried out at RT.

III. RESULTS AND DISCUSSION

Figure 1(a) indicates a typical SPL spectrum of sample S1 with $P = 89$ W/cm^2, where the experimental scheme of the SPL is shown in Fig. 1(b). In this experiment, PL photons emitted from the sample surface were collimated and transferred by an off-axis parabolic mirror to the detecting system via a collecting lens with an effective NA of 0.20. The SPL spectrum shows a single-peak form with the peak photon energy $E_{peak}^{SPL} = 2.264$ eV. By contrast, the ODPL spectrum shown in Fig. 1(c) gives a two-peak structure, where the experimental setup is schematically illustrated in Fig. 1(d). One of the maximum energies $\left(E_{peak}^{ODPL,H}\right)$ is located at 2.267 eV, which is close to E_{peak}^{SPL} of 2.264 eV, and the other is at 2.158 eV ($=E_{peak}^{ODPL,L}$). Such a two-peak structure in ODPL spectra is commonly observed in direct bandgap materials such as GaN[26] and ZnO,[27] where E_{abs}

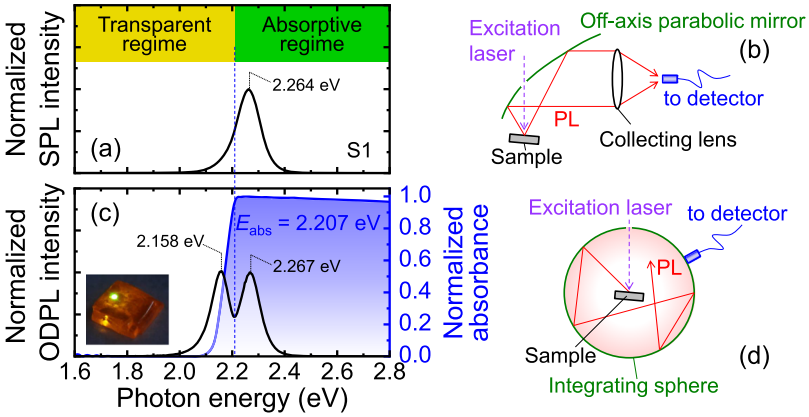

FIG. 1. (a) A typical SPL spectrum of sample S1 and (b) schematic of the SPL measurement. (c) A typical ODPL spectrum of sample S1 and (d) schematic of the ODPL measurement. The inset in Fig. 1(c) indicates appearance of a bulk $MAPbBr_3$ crystal under the illumination of the excitation laser, where green emission ($E > E_{abs}$) occurs as a spot and yellow emission and orange emission ($E < E_{abs}$) are seen in the entire crystal.

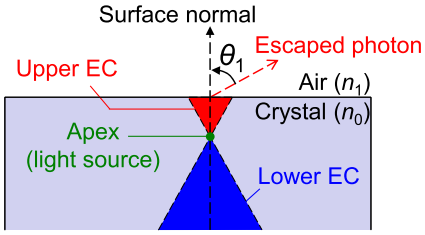

FIG. 3. The escaping cone (EC), which has a double-cone structure (upper and lower cones) with a common apex as a point light source.

matched with the local minimum energy of the two-peak spectrum. We note that there are several publications in which PL spectra exhibiting a shoulder with E of a few tens of meV lower than E_{peak}^{SPL} were attributed to the polar fluctuation,[29] mixed phases,[30] and excitons with different binding energies.[31] However, the energy difference between $E_{peak}^{ODPL,H}$ and $E_{peak}^{ODPL,L}$ is as large as 109 meV, which cannot be accounted for by the above mechanisms. Moreover, such two-peak spectra are commonly observed in direct bandgap materials but not in single-crystalline phosphors and indirect bandgap materials such as h-BN because of their sufficiently separated emission and absorption energy bands. Above E_{abs}, a crystal behaves as an absorptive medium for PL photons. Similar to the cases of GaN and ZnO, absorbance of the $MAPbBr_3$ crystal is quickly elevated with E around E_{abs} = 2.207 eV, as shown in Fig. 1(c). Therefore, the PL photons with $E > E_{abs}$ must be emitted from the crystal via an upper escaping cone (EC). The EC has a double-cone structure with a common apex, which is a point light source, and consists of the upper and lower cones, as shown in Fig. 3. However, the lower EC cannot contribute as an escaping channel for PL photons with $E > E_{abs}$ due to the sample thickness (sub-millimeter). By contrast, PL photons with $E < E_{abs}$ can travel inside the crystal; therefore, escaping channel is not limited by the EC. Actually, green emission ($E > E_{abs}$) can be observed as the excitation spot, and yellow and orange emission ($E < E_{abs}$) can be seen in the entire crystal, as indicated in the inset of Fig. 1(c). Since the photodetection is done via the upper EC in SPL spectroscopy while the ODPL setup can omnidirectionally observe PL photons, detection probability of photons with $E < E_{abs}$ is much higher in the ODPL setup than in case of the SPL, resulting in the formation of the additional lower peak $E_{peak}^{ODPL,L}$ in ODPL spectra. In short, LEE is much higher for $E < E_{abs}$ than that for $E > E_{abs}$, and the origin of the two-peak ODPL spectra is the strong E-dependence of LEE.

To accentuate differences in the spatial distribution of escaped PL photons with E below and above E_{abs}, ARPL spectroscopy was then performed. The detecting photon energy (E_{det}) was set to be 2.01 eV, 2.16 eV, and 2.30 eV. Figure 4(a) represents PL intensity distribution with different E_{det}. The excitation laser was irradiated from the front surface of the sample, where the photo-excitation density (P) is kept to be 0.38 W/cm^2. The angle θ_1 indicates a relative angle between the sample and an optical fiber connecting to the detecting system, where an angle θ_1 = 0° (180°) is defined as the normal to the front (back) surface of the crystal. The sample crystal was mounted on a motorized rotation stage, and θ_1 can be controlled, as shown in Fig. 2. The ARPL spectra detected from the front and back surfaces are shown in Figs. 4(b) and 4(c), respectively. The ARPL spectrum with θ_1 = 0°, observed along normal to the front surface represented in Fig. 4(b), shows a single-peak form with a peak E of 2.264 eV. This spectrum corresponds to the spectral shape of the SPL measurements [Fig. 1(a)]. PL intensity with E_{det} = 2.30 eV ($>E_{abs}$) decreases with the increase in θ_1 and reached nearly zero when θ_1 = 90°. However, PL intensities with E_{det} = 2.01 eV and 2.16 eV ($<E_{abs}$) have nonzero values even for θ_1 = 90°, and the peak ARPL intensity is given with E = 2.16 eV, which matched with $E_{peak}^{ODPL,L}$. Since ODPL is angle-integrating PL spectroscopy, the origin of the double-peak spectral form can be reconfirmed, that is, the existence of E_{abs} within the bandwidth of spontaneous emission spectra in the crystal. We note that the distribution pattern of emitted light with $E < E_{abs}$ depends on the sample shape. Since the sample crystals are not perfectly cubic shape, the pattern is asymmetric.

The distribution of ARPL intensity E_{det} = 2.30 eV becomes nearly perfect Lambertian distribution, as shown in Fig. 4(a), although ARPL intensities with E_{det} = 2.01 eV and 2.16 eV show sample-dependent and asymmetric distribution. Lambertian distribution of light is caused from the upper EC, as shown in the Appendix, and can strongly support our assumption where escaping channel for PL photons with $E > E_{abs}$ is strictly limited by the upper EC without multiple reflection and long travel inside the crystal. This fact helps the LEE calculation to be easy and reliable. In an extreme case, the repeatable and reliable IQE quantification is possible, even when a sample crystal is placed outside an integrating sphere[32] by

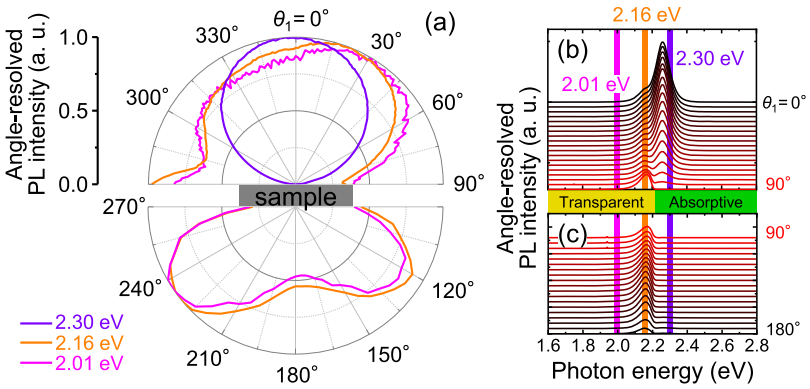

FIG. 4. (a) The PL intensity distribution measured by ARPL spectroscopy with different E_{det}. The ARPL spectra, which were detected from (b) front surface and (c) back surface, are also shown.

the Lambertian distribution of light propagating to only the upper direction with $E > E_{abs}$.

The EQE value shown in Fig. 5(a) tends to be monotonically elevated by the increment of P, and sample S3 gives larger EQE. The maximum EQE was observed in S3 to be 11.3% with $P = 10$ W/cm^2. However, further increment of P induces the depression of EQE. We note that this EQE depression is a reversible phenomenon, and therefore, it should not be caused from eternal damages. To directly correlate material properties with optical response, IQE rather than EQE is straight forward. By the procedure proposed in Ref. 25, the EQE values can be converted to IQE via "direct EQE." The direct EQE (ξ'), of which the escaping channel is limited by the upper EC, can be given by

$$\xi' = \frac{1 + \kappa\delta_{SPL}}{1 + \delta_{ODPL}}\xi, \tag{1}$$

where ξ represents experimentally obtained EQE, as shown in Fig. 5(a), and δ is a ratio of the spectral area with $E < E_{abs}$ to that with $E > E_{abs}$. κ is a correction parameter to compensate the dispersion of n_1 around E_{abs} and usually takes a constant around unity. As stated above, the entire spectrum of SPL and the partial spectrum of ODPL with $E > E_{abs}$ are commonly originated from PL photons escaped via the upper EC; therefore, the factor $1 + \delta_{SPL}/1 + \delta_{ODPL}$ represents a ratio between the number of PL photons escaped via the upper EC and the total number of PL photons, of which the escaping channel is unlimited. The parameters δ_{SPL}, δ_{ODPL}, and ξ can be experimentally determined by SPL and ODPL spectroscopy; therefore, direct EQE, ξ', can be derived without any theoretical analysis. Since LEE via the upper EC (ζ) is calculated by considering the volume of the upper EC and the Fresnel transmission (T) from matter to air,

$$\zeta = \int_0^{\theta_c} \frac{2\pi \sin\theta_0}{4\pi} \frac{T_P(\theta_0) + T_S(\theta_0)}{2} d\theta_0, \tag{2}$$

where T is averaged between P- and S-polarizations and θ_c represents the critical angle. The angle θ_0 indicates an angle between the propagation direction of light inside the crystal and the surface normal. Here, the refractive index of the bulk $MAPbBr_3$ crystal around the energy of NBE emission is 2.45,[33] and thus, ζ was calculated to be 3.40% according to Eq. (2). By using ξ' and ζ, the IQE value (η) can be quantified by considering the photon recycling[25] as

$$\eta = \frac{\xi'}{\zeta + (1 - \zeta)\xi'}, \tag{3}$$

where quantified IQE is plotted in Fig. 5(b). Similar to the trend of EQE, IQE was elevated for P, and sample S3 gave larger IQE. Such monotonic increment of IQE for P was also observed for the NBE emission in other inorganic semiconductors such as GaN[26] and ZnO.[27] In these cases of wide bandgap materials, the IQE elevation is accompanied with the elongation PL lifetime. Therefore, the origin of the IQE elevation can be the saturation of nonradiative recombination centers (NRCs). However, in the case of bulk $MAPbBr_3$ crystals, PL lifetime was reported to be shortened for P.[18] This fact suggests that the acceleration of radiative process mainly occurs in bulk $MAPbBr_3$ crystals.

Further increment of P induces the depression of IQE. In S3, a slight blue-shift was observed for $P > 28$ W/cm^2, as indicated in Fig. 6, and it suggests the band-filling effect where carrier concentration is large enough to shift the quasi-Fermi levels. In this case, the Auger recombination processes should be considered as nonradiative many-body effects. Yang *et al.* reported the coefficients A, B, and C corresponding to nonradiative monoparticle, radiative biparticle, and nonradiative triparticle recombination processes to be 2.7×10^7 s^{-1}, 4.9×10^{-10} cm^3 s^{-1}, and 1.4×10^{-28} cm^6 s^{-1}, respectively, under the simple model.[34] According to that, theoretical IQE (η^{calc}) can be calculated as

$$\eta^{calc}(N) = \frac{BN^2}{AN + BN^2 + CN^3}, \tag{4}$$

and the characteristic carrier concentration N_{max}^{calc}, which gives the maximum η^{calc} (η_{max}^{calc}), can be analytically evaluated by the first derivation of Eq. (4) to be

$$N_{max}^{calc} = \sqrt{\frac{A}{C}} = 1.4 \times 10^{17}\ \text{cm}^{-3}, \tag{5}$$

where $\eta_{max}^{calc} = 0.56$. On the other hand, we experimentally obtained the maximum IQE (η_{max}) to be 0.63 under $P = 28$ W/cm^2, which corresponds the photo-excitation rate (G) as $G = 5.7 \times 10^{19}$ cm^{-2} s^{-1}.

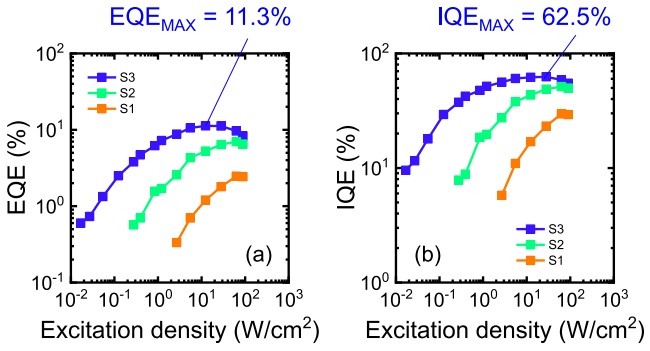

FIG. 5. (a) The EQE and (b) IQE curves of the samples as functions of the photo-excitation density (P).

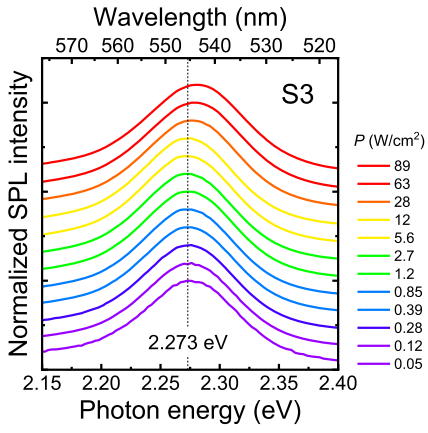

FIG. 6. The SPL spectra of sample S3 with different P.

Since the coefficient A depends on the concentration of NRCs, we tried to find appropriate value of A to equalize η_{max}^{calc} with η_{max} and got $A = 1.5 \times 10^7\ s^{-1}$, where $N_{max}^{calc} = 1.1 \times 10^{17}\ cm^{-3}$.

To obtain a broad outline, we made a rough estimation by assuming that the penetration depth (d_{exc}) of the excitation laser (3.06 eV) is 100 nm[35] and the quasi-equilibrium condition under cw-excitation. The excited carrier concentration (N) can be estimated by the relationship between G and N as

$$G/d_{exc} = AN + BN^2 + CN^3, \tag{6}$$

where N can be derived to be $0.78 \times 10^{17}\ cm^{-3}$ for $P = 28\ W/cm^2$. Since $N = 0.78 \times 10^{17}\ cm^{-3}$ obtained by Eq. (6) and $N_{max}^{calc} = 1.1 \times 10^{17}\ cm^{-3}$ derived from Eq. (5) with $A = 1.5 \times 10^7\ s^{-1}$ are similar, the simple model based on A, B, and C coefficients may roughly reproduce the experimental results. Therefore, the prime suspect of the IQE suppression for $P > 28\ W/cm^2$ should be the Auger recombination processes. The differences between experiments and calculations can be due to volume averaging, where the IQE value quantified by ODPL spectroscopy is a sort of volume-averaged quantity with inhomogeneous excitation along the in-plane and the depth directions. Actually, a microscopic PL experiment[20] gave larger IQE. Long carrier diffusion length, which is the distinctive feature of halide perovskites,[5,17,18] is also a factor to be considered. According to the P-dependence of IQE, photo-excited carriers can migrate to the position with lower local IQE. In this manner, experimentally obtained IQE should be smaller compared with no diffusion limit. In other words, IQE quantified by ODPL spectroscopy is potentially a lower limit value of IQE. Further studies should be done to precisely correlate the experiments with theoretical models considering the microscopic processes.

Finally, it should be mentioned that the IQE is significantly enhanced by changing the MABr concentrations when the sample were grown as shown in Fig. 5(b), indicating that NRCs correlating with the cation vacancies dominate the nonradiative recombination processes. Actually, divacancies composed of anion and cation vacancies are realized to be the intrinsic NRCs in GaN.[36] Our finding suggests that further improvement of IQE can be achieved by optimization of the crystal fabrication process to minimize the formation of cation-vacancy-related point defects.

IV. CONCLUSION

The IQE values of bulk $MAPbBr_3$ crystals were experimentally quantified by ODPL spectroscopy. The ARPL measurement revealed that the PL with E higher than E_{abs} shows a Lambertian distribution. Therefore, the extraction efficiency for that is strictly determined by the upper EC, which secures the validity of the IQE quantification by ODPL spectroscopy. The IQE value strongly depends on P, and the $MAPbBr_3$ crystal fabricated with MA-rich condition gave the maximum IQE of 62.5% under $P = 28\ W/cm^2$. Further elevation of P induced the depression of IQE due to the Auger effects.

ACKNOWLEDGMENTS

This work was partly supported by the Five-Star Alliance, JSPS KAKENHI (Grant Nos. JP16H06427, JP17H02907, and JP17H04809), and JST-CREST (Grant No. JPMJCR16N3), Japan. We thank Dr. T. Yamada for useful discussions.

APPENDIX: LAMBERTIAN

1. Origin of Lambertian

Photon flux (F) from a point light source inside a material has a relationship with spectral irradiance (I) which is obtained by the detecting system existing outside of the material,

$$F = \int_A \int_\lambda I(\lambda) \mathrm{d}\lambda \mathrm{d}A,$$

where λ and A are the wavelength of the light and the surface area of the closed space including the source. In a polar coordinate system (r, θ, φ) having the source as the origin, I inside the crystal becomes

$$I_0 = \frac{F(\theta_0)}{4\pi r^2}.$$

On the other hand, I outside the crystal can be given as

$$I_1 = I_0 \frac{\mathrm{d}S_0}{\mathrm{d}S_1}$$

because

$$F = \int_{A_1} \int_\lambda I_1(\lambda) \mathrm{d}\lambda \mathrm{d}S_1 = \int_{A_0} \int_\lambda I_0(\lambda) \mathrm{d}\lambda \mathrm{d}S_0$$
$$= \int_{A_1} \int_\lambda I_1(\lambda) \mathrm{d}\lambda \frac{\mathrm{d}S_0}{\mathrm{d}S_1} \mathrm{d}S_1,$$

where the indices 0 and 1 represent inside and outside the crystal, respectively, and S is the surface element of a unit sphere. Therefore, the relationship between I_1 and I_0 will be clear when $\frac{\mathrm{d}S_0}{\mathrm{d}S_1}$ is known.

Snell's law gives

$$n_1 \sin\theta_1 = n_0 \sin\theta_0;$$

therefore, the angle difference ($\mathrm{d}\theta_0$) of light in the crystal induces the angle variation of that outside the crystal ($\mathrm{d}\theta_1$) as

$$n_1 \cos\theta_1 \frac{\mathrm{d}\theta_1}{\mathrm{d}\theta_0} = n_0 \cos\theta_0,$$

$$\therefore \mathrm{d}\theta_1 = \frac{n_0}{n_1} \frac{\cos\theta_0}{\cos\theta_1} \mathrm{d}\theta_0.$$

Spectral photon flux should be the same in the small variations of $\mathrm{d}\theta_0$ and $\mathrm{d}\theta_1$, and thus,

$$I_0 \mathrm{d}A_0 = I_1 \mathrm{d}A_1,$$

where $A = 2\pi S$ is an areal element of spherical zone given by the integration of S around φ. Defining $\mathrm{d}A$ between θ and $\theta + \mathrm{d}\theta$ as

$$\mathrm{d}A = 2\pi r \sin\theta\ r\mathrm{d}\theta,$$

$\mathrm{d}A$ outside and inside the crystal, respectively, become

$$\mathrm{d}A_1 = 2\pi r \sin\theta_1\ r\mathrm{d}\theta_1 = 2\pi r \left(\frac{n_0}{n_1} \sin\theta_0\right) r \left(\frac{n_0}{n_1} \frac{\cos\theta_0}{\cos\theta_1} \mathrm{d}\theta_0\right)$$
$$= 2\pi r^2 \left(\frac{n_0}{n_1}\right)^2 \frac{\cos\theta_0}{\cos\theta_1} \sin\theta_0 \mathrm{d}\theta_0$$

and

$$\mathrm{d}A_0 = 2\pi r \sin\theta_0\ r\mathrm{d}\theta_0 = 2\pi r^2 \sin\theta_0\ \mathrm{d}\theta_0.$$

Then, we get

$$\frac{dA_0}{dA_1} = \left(\frac{n_1}{n_0}\right)^2 \frac{\cos\theta_1}{\cos\theta_0} = \left(\frac{n_1}{n_0}\right)^2 \frac{\cos\theta_1}{\sqrt{1-\left(\frac{n_1}{n_0}\right)^2 \sin^2\theta_1}}.$$

Here, $\cos\theta_1$ appears in the relationship between dA_0 and dA_1. Actually, a factor of $\sqrt{1-\left(\frac{n_1}{n_0}\right)^2 \sin^2\theta_1}$ will make the light distribution slightly broader but is not important for relatively high index materials, because $\sin \to 0$, and $\cos \to 1$ when $n_1 \gg n_0$. This approximation gives

$$\frac{dA_0}{dA_1} = \left(\frac{n_1}{n_0}\right)^2 \frac{\cos\theta_1}{\sqrt{1-\left(\frac{n_1}{n_0}\right)^2 \sin^2\theta_1}} \sim \left(\frac{n_1}{n_0}\right)^2 \cos\theta_1.$$

In this case, spectral irradiance obtained by the detecting system existing outside of the material becomes

$$I_1 = I_0 \frac{dA_0}{dA_1} = \frac{P}{4\pi r^2}\left(\frac{n_1}{n_0}\right)^2 \frac{\cos\theta_1}{\sqrt{1-\left(\frac{n_1}{n_0}\right)^2 \sin^2\theta_1}} \sim \frac{P}{4\pi r^2}\left(\frac{n_1}{n_0}\right)^2 \cos\theta_1,$$

where I_1 is proportional to $\cos\theta_1$.

REFERENCES

[1] A. Kojima, K. Teshima, Y. Shirai, and T. Miyasaka, J. Am. Chem. Soc. **131**, 6050 (2009).
[2] S. D. Stranks, G. E. Eperon, G. Grancini, C. Menelaou, M. J. P. Alcocer, T. Leijtens, L. M. Herz, A. Petrozza, and H. J. Snaith, Science **342**, 341 (2013).
[3] Y. Yamada, T. Nakamura, M. Endo, A. Wakamiya, and Y. Kanemitsu, Appl. Phys. Express **7**, 032302 (2014).
[4] G. Maculan, A. D. Sheikh, A. L. Abdelhady, M. I. Saidaminov, M. A. Haque, B. Murali, E. Alarousu, O. F. Mohammed, T. Wu, and O. M. Bakr, J. Phys. Chem. Lett. **6**, 3781 (2015).
[5] Y. Yang, Y. Yan, M. Yang, S. Choi, K. Zhu, J. M. Luther, and M. C. Beard, Nat. Commun. **6**, 7961 (2015).
[6] A. Sadhanala, S. Ahmad, B. Zhao, N. Giesbrecht, P. M. Pearce, F. Deschler, R. L. Z. Hoye, K. C. Gödel, T. Bein, P. Docampo, S. E. Dutton, M. F. L. De Volder, and R. H. Friend, Nano Lett. **15**, 6095 (2015).
[7] M. Saliba, T. Matsui, K. Domanski, J.-Y. Seo, A. Ummadisingu, S. M. Zakeeruddin, J.-P. Correa-Baena, W. R. Tress, A. Abate, A. Hagfeldt, and M. Grätzel, Science **354**, 206 (2016).
[8] A. Priyadarsh, L. J. Haur, P. Murray, D. Fu, S. Kulkarni, G. Xing, T. C. Sum, N. Mathews, and S. G. Mhaisalkar, Energy Environ. Sci. **9**, 3687 (2016).
[9] L. M. Pazos-Outón, M. Szumilo, R. Lamboll, J. M. Richter, M. Crespo-Quesada, M. Abdi-Jalebi, H. J. Beeson, M. Vrućinić, M. Alsari, H. J. Snaith, B. Ehrler, R. H. Friend, and F. Deschler, Science **351**, 1430 (2016).
[10] S. A. Veldhuis, P. P. Boix, N. Yantara, M. Li, T. C. Sum, N. Mathews, and S. G. Mhaisalkar, Adv. Mater. **28**, 6804 (2016).
[11] E. Zheng, B. Yuh, G. A. Tosado, and Q. Yu, J. Mater. Chem. C **5**, 3796 (2017).
[12] Z. Xiao, R. A. Kerner, L. Zhao, N. L. Tran, K. M. Lee, T.-W. Koh, G. D. Scholes, and B. P. Rand, Nat. Photonics **11**, 108 (2017).
[13] S. De Wolf, J. Holovsky, S.-J. Moon, P. Löper, B. Niesen, M. Ledinsky, F.-J. Haug, J.-H. Yum, and C. Ballif, J. Phys. Chem. Lett. **5**, 1035 (2014).
[14] Q. Dong, Y. Fang, Y. Shao, P. Mulligan, J. Qiu, L. Cao, and J. Huang, Science **347**, 967 (2015).
[15] O. D. Miller, E. Yablonovitch, and S. R. Kurtz, IEEE J. Photovoltaics **2**, 303 (2012).
[16] L. Zhu, T. Mochizuki, M. Yoshita, S. Chen, C. Kim, H. Akiyama, and Y. Kanemitsu, Opt. Express **24**, A740 (2016).
[17] Y. Yamada, T. Yamada, L. Q. Phuong, N. Maruyama, H. Nishimura, A. Wakamiya, Y. Murata, and Y. Kanemitsu, J. Am. Chem. Soc. **137**, 10456 (2015).
[18] T. Yamada, Y. Yamada, H. Nishimura, Y. Nakaike, A. Wakamiya, Y. Murata, and Y. Kanemitsu, Adv. Electron. Mater. **2016**, 1500290.
[19] T. Yamada, T. Aharen, and Y. Kanemitsu, Phys. Rev. Lett. **120**, 057404 (2018).
[20] T. Yamada, Y. Yamada, Y. Nakaike, A. Wakamiya, and Y. Kanemitsu, Phys. Rev. Appl. **7**, 014001 (2017).
[21] Y. Yamada, T. Yamada, and Y. Kanemitsu, Bull. Chem. Soc. Jpn. **90**, 1129 (2017).
[22] S.-T. Ha, C. Shen, J. Zhang, and Q. Xiong, Nat. Photonics **10**, 115 (2016).
[23] T. Yamada, T. Aharen, and Y. Kanemitsu, Phys. Rev. Mater. **3**, 024601 (2019).
[24] J. M. Richter, M. Abdi-Jalebi, A. Sadhanala, M. Tabachnyk, J. P. H. Rivett, L. M. P. Outón, K. C. Gödel, M. Price, F. Deschler, and R. H. Friend, Nat. Commun. **7**, 13941 (2016).
[25] K. Kojima, T. Ohtomo, K. Ikemura, Y. Yamazaki, M. Saito, H. Ikeda, K. Fujito, and S. F. Chichibu, J. Appl. Phys. **120**, 015704 (2016).
[26] K. Kojima, H. Ikeda, K. Fujito, and S. F. Chichibu, Appl. Phys. Lett. **111**, 032111 (2017).
[27] K. Kojima, T. Harada, A. Tsukazaki, and S. F. Chichibu, in The 9th International Workshop on ZnO and Related Materials (IWZnO), MA5, 2016.
[28] D. Shi, V. Adinolfi, R. Comin, M. Yuan, E. Alarousu, A. Buin, Y. Chen, S. Hoogland, A. Rothenberger, K. Katsiev, Y. Losovyj, X. Zhang, P. A. Dowben, O. F. Mohammed, E. H. Sargent, and O. M. Bakr, Science **347**, 519 (2015).
[29] B. Wu, H. Yuan, Q. Xu, J. A. Steele, D. Giovanni, P. Puech, J. Fu, Y. F. Ng, N. F. Jamaludin, A. Solanki, S. Mhaisalkar, N. Mathews, M. B. J. Roeffaers, M. Grätzel, J. Hofkens, and T. C. Sum, Nat. Commun. **10**, 484 (2019).
[30] D. Niesner, O. Schuster, M. Wilhelm, I. Levchuk, A. Osvet, S. Shrestha, M. Batentschuk, C. Brabec, and T. Fauster, Phys. Rev. B **95**, 075207 (2017).
[31] T. T. H. Do, A. G. del Águila, C. Cui, J. Xing, Z. Ning, and Q. Xiong, Phys. Rev. B **96**, 075308 (2017).
[32] K. Kojima, K. Ikemura, and S. F. Chichibu, Appl. Phys. Express **12**, 062010 (2019).
[33] M. Kato, T. Fujiseki, T. Miyadera, T. Sugita, S. Fujimoto, M. Tamakoshi, M. Chikamatsu, and H. Fujiwara, J. Appl. Phys. **121**, 115501 (2017).
[34] Y. Yang, M. Yang, Z. Li, R. Crisp, K. Zhu, and M. C. Beard, J. Phys. Chem. Lett. **6**, 4688 (2015).
[35] J. S. Park, S. Choi, Y. Yan, Y. Yang, J. M. Luther, S. H. Wei, P. Parilla, and K. Zhu, J. Phys. Chem. Lett. **6**, 4304 (2015).
[36] S. F. Chichibu, A. Uedono, K. Kojima, H. Ikeda, K. Fujito, S. Takashima, M. Edo, K. Ueno, and S. Ishibashi, J. Appl. Phys. **123**, 161413 (2018).